Euclid commissioning results: the Near Infrared Spectrometer and Photometer (NISP) signal detection chain

On behalf of the Euclid Collaboration: F. Cogato [*1,2], E. Medinaceli[2], R. Barbier[3], S. Dusini[4], W. Gillard[5], K. Jahnke[6], E. Prieto[7], N. Auricchio[2], E. Balbi[8], A. Balestra[9], P. Battaglia[2], D. Bonino[10], V. Capobianco[10], R. Chary[11,12], S. Conseil[3], L. Corcione[10], G. Delucchi[13,8], R. Farinelli[2], S. Ferriol[3], E. Franceschi[2], L. Gabarra[14], F. Gianotti[2], F. Grupp[15,16], E. Lentini[17], S. Ligori[10], G. Morgante[2], K. Paterson[6], E. Romelli[18], L. Sauniere[5], M. Schirmer[6], C. Sirignano[19,4], G. Sirri[20], G. Testera[8], M. Trifoglio[2], A. Troja[19,4], L. Valenziano[5,20], Y. Copin[3], M. Frailis[18], B. Kubik[3], M. Scodeggio[21], J.-C. Barriere[22], M. Berthe[23], C. Bodendorf[15], A. Caillat[7], M. Carle[7], R. Casas[24,25], H. Cho[26], A. Costille[7], F. Ducret[7], B. Garilli[21], W. Holmes[26], F. Hormuth[27], A. Hornstrup[28,29], M. Jhabvala[30], R. Kohley[31], D. Le Mignant[7], P. B. Lilje[32], I. Lloro[33], C. Padilla[34], G. Polenta[35], J.-C. Salvignol[36], G. Seidel[6], B. Serra[37], A. Secroun[5], G. Smadja[3], L. Stanco[4], P. Strada[36], R. Toledo-Moreo[38], S. Anselmi[4,19,39], E. Borsato[19,4], L. Caillat[5], C. Colodro-Conde[40], V. Conforti[2], J. E. Davies[6], A. Renzi[19,4], F. Dal Corso[4], S. Davini[8], A. Derosa[2], J. J. Diaz[41], S. Di Domizio[13,8], D. Di Ferdinando[42], A. G. Ferrari[43,42], F. Fornari[20], F. Giacomini[42], O. Krause[6], F. Laudisio[4], J. Macias-Perez[44], J. Marpaud[44], N. Mauri[43,42], R. da Silva[45,35], M. Niclas[5], F. Passalacqua[19,4], I. Risso[17], P. Lagier[5], A. N. Sorensen[46], P. Stassi[44], J. Steinwagner[15], M. Tenti[42], C. Thizy[47], S. Tosi[13,8], R. Travaglini[42], O. Tubio[40], C. Valieri[42], S. Ventura[4], C. Vescovi[44], and J. Zoubian[5]

[1]Dipartimento di Fisica e Astronomia "Augusto Righi" - Alma Mater Studiorum Università di Bologna, via Piero Gobetti 93/2, 40129 Bologna, Italy
[2]INAF-Osservatorio di Astrofisica e Scienza dello Spazio di Bologna, Via Piero Gobetti 93/3, 40129 Bologna, Italy
[3]Université Claude Bernard Lyon 1, CNRS/IN2P3, IP2I Lyon, UMR 5822, Villeurbanne, F-69100, France
[4]INFN-Padova, Via Marzolo 8, 35131 Padova, Italy
[5]Aix-Marseille Université, CNRS/IN2P3, CPPM, Marseille, France
[6]Max-Planck-Institut für Astronomie, Königstuhl 17, 69117 Heidelberg, Germany
[7]Aix-Marseille Université, CNRS, CNES, LAM, Marseille, France
[8]INFN-Sezione di Genova, Via Dodecaneso 33, 16146, Genova, Italy
[9]INAF-Osservatorio Astronomico di Padova, Via dell'Osservatorio 5, 35122 Padova, Italy
[10]INAF-Osservatorio Astrofisico di Torino, Via Osservatorio 20, 10025 Pino Torinese (TO), Italy
[11]Infrared Processing and Analysis Center, California Institute of Technology, Pasadena, CA 91125, USA
[12]University of California, Los Angeles, CA 90095-1562, USA
[13]Dipartimento di Fisica, Università di Genova, Via Dodecaneso 33, 16146, Genova, Italy
[14]Department of Physics, Oxford University, Keble Road, Oxford OX1 3RH, UK
[15]Max Planck Institute for Extraterrestrial Physics, Giessenbachstr. 1, 85748 Garching, Germany
[16]Universitäts-Sternwarte München, Fakultät für Physik, Ludwig-Maximilians-Universität München, Scheinerstrasse 1, 81679 München, Germany
[17]Dipartimento di Fisica, Università degli studi di Genova, and INFN-Sezione di Genova, via Dodecaneso 33, 16146, Genova, Italy
[18]INAF-Osservatorio Astronomico di Trieste, Via G. B. Tiepolo 11, 34143 Trieste, Italy
[19]Dipartimento di Fisica e Astronomia "G. Galilei", Università di Padova, Via Marzolo 8, 35131 Padova, Italy
[20]INFN-Bologna, Via Irnerio 46, 40126 Bologna, Italy
[21]INAF-IASF Milano, Via Alfonso Corti 12, 20133 Milano, Italy
[22]CEA-Saclay, DRF/IRFU, departement d'ingenierie des systemes, bat472, 91191 Gif sur Yvette cedex, France
[23]Université Paris-Saclay, Université Paris Cité, CEA, CNRS, AIM, 91191, Gif-sur-Yvette, France

Space Telescopes and Instrumentation 2024: Optical, Infrared, and Millimeter Wave, edited by Laura E. Coyle, Shuji Matsuura, Marshall D. Perrin, Proc. of SPIE Vol. 13092, 130923G · © 2024 SPIE · 0277-786X · doi: 10.1117/12.3017952

[24]Institut d'Estudis Espacials de Catalunya (IEEC), Edifici RDIT, Campus UPC, 08860 Castelldefels, Barcelona, Spain
[25]Institute of Space Sciences (ICE, CSIC), Campus UAB, Carrer de Can Magrans, s/n, 08193 Barcelona, Spain
[26]Jet Propulsion Laboratory, California Institute of Technology, 4800 Oak Grove Drive, Pasadena, CA, 91109, USA
[27]Felix Hormuth Engineering, Goethestr. 17, 69181 Leimen, Germany
[28]Technical University of Denmark, Elektrovej 327, 2800 Kgs. Lyngby, Denmark
[29]Cosmic Dawn Center (DAWN), Denmark
[30]NASA Goddard Space Flight Center, Greenbelt, MD 20771, USA
[31]ESAC/ESA, Camino Bajo del Castillo, s/n., Urb. Villafranca del Castillo, 28692 Villanueva de la Cañada, Madrid, Spain
[32]Institute of Theoretical Astrophysics, University of Oslo, P.O. Box 1029 Blindern, 0315 Oslo, Norway
[33]NOVA optical infrared instrumentation group at ASTRON, Oude Hoogeveensedijk 4, 7991PD, Dwingeloo, The Netherlands
[34]Institut de Física d'Altes Energies (IFAE), The Barcelona Institute of Science and Technology, Campus UAB, 08193 Bellaterra (Barcelona), Spain
[35]Space Science Data Center, Italian Space Agency, via del Politecnico snc, 00133 Roma, Italy
[36]European Space Agency/ESTEC, Keplerlaan 1, 2201 AZ Noordwijk, The Netherlands
[37]European Southern Observatory, Karl-Schwarzschild Str. 2, 85748 Garching, Germany
[38]Universidad Politécnica de Cartagena, Departamento de Electrónica y Tecnología de Computadoras, Plaza del Hospital 1, 30202 Cartagena, Spain
[39]Laboratoire Univers et Théorie, Observatoire de Paris, Université PSL, Université Paris Cité, CNRS, 92190 Meudon, France
[40]Instituto de Astrofísica de Canarias, Calle Vía Láctea s/n, 38204, San Cristóbal de La Laguna, Tenerife, Spain
[41]Instituto de Astrofísica de Canarias (IAC); Departamento de Astrofísica, Universidad de La Laguna (ULL), 38200, La Laguna, Tenerife, Spain
[42]INFN-Sezione di Bologna, Viale Berti Pichat 6/2, 40127 Bologna, Italy
[43]Dipartimento di Fisica e Astronomia "Augusto Righi" - Alma Mater Studiorum Università di Bologna, Viale Berti Pichat 6/2, 40127 Bologna, Italy
[44]Univ. Grenoble Alpes, CNRS, Grenoble INP, LPSC-IN2P3, 53, Avenue des Martyrs, 38000, Grenoble, France
[45]INAF-Osservatorio Astronomico di Roma, Via Frascati 33, 00078 Monteporzio Catone, Italy
[46]Niels Bohr Institute, University of Copenhagen, Jagtvej 128, 2200 Copenhagen, Denmark
[47]Centre Spatial de Liege, Universite de Liege, Avenue du Pre Aily, 4031 Angleur, Belgium

ABSTRACT

Euclid, the M2 mission of the ESA's Cosmic Vision 2015-2025 program, aims to explore the Dark Universe by conducting a survey of approximately 14 000 deg^2 and creating a 3D map of the observable Universe of around 1.5 billion galaxies up to redshift $z \sim 2$. This mission uses two main cosmological probes: weak gravitational lensing and galaxy clustering, leveraging the high-resolution imaging capabilities of the Visual Imaging (VIS) instrument and the photometric and spectroscopic measurements of the Near Infrared Spectrometer and Photometer (NISP) instrument. This paper details some of the activities performed during the commissioning phase of the NISP instrument, following the launch of *Euclid* on July 1, 2023. In particular, we focus on the calibration of the NISP detectors' baseline and on the performance of a parameter provided by the onboard data processing (called NISP Quality Factor, QF) in detecting the variability of the flux of cosmic rays hitting the NISP detectors. The NISP focal plane hosts sixteen Teledyne HAWAII-2RG (H2RG) detectors. The calibration of these detectors includes the baseline optimization, which optimizes the dynamic range and stability of the signal acquisition. Additionally, this paper investigates the impact of Solar proton flux on the NISP QF, particularly during periods of high Solar activity. Applying a selection criterion on the QF (called NISP QF Proxy), the excess counts are used to monitor the amount of charged particles hitting the NISP detectors. A good correlation was found between the Solar proton flux component above 30 MeV and the NISP QF Proxy, revealing that NISP detectors are not subject to the lower energy components, which are absorbed by the shielding provided by the spacecraft.

Keywords: *Euclid*, NISP, Quality Factor, Near-Infrared Detectors, H2RG, Cosmic Rays

* fabrizio.cogato@inaf.it

1. INTRODUCTION

Euclid is the M2 mission of the European Space Agency (ESA) Cosmic Vision 2015-2025 program, designed to explore the composition and evolution of the Dark Universe through a 14 000 deg^2 survey campaign that will provide a 3D map of about 1.5 billion galaxies up to redshift $z \sim 2$ [1]. To achieve such an ambitious scientific goal, *Euclid* exploits two main cosmological probes: weak gravitational lensing and galaxy clustering. The study of these two statistical properties of the observable Universe will be made possible by the combined efforts of the two instruments that place *Euclid* at the forefront of cosmological survey missions. In practice, the Visible imaging (VIS) instrument [2] enables high-resolution imaging to measure the distribution of matter in distant galaxies, while the Near-Infrared Spectrometer and Photometer (NISP) instrument [3] measures their photometric and spectroscopic redshift to map the distribution of galaxies in space-time.

A detailed overview of the *Euclid* mission, with the complexity of its design, subsystems, operations and science data management is reported in the dedicated literature. This work describes part of the activities performed during the NISP commissioning, in the first months after the launch of *Euclid* on July 1, 2023.

In particular, we focus on the effort made to accurately calibrate the baseline of the NISP detectors (Sect. 3.1) and to verify the performance of the Quality Factor parameter, which provides an estimate of the quality of the onboard NISP data processing. In particular, by applying a selection criterion to the NISP QF distribution, the sensitivity of NISP detectors to Solar proton flux is estimated (Sect. 3.2).

2. BRIEF DESCRIPTION OF THE NISP INSTRUMENT

For the purposes of this analysis, the NISP instrument is schematically divided into three main subsystems: the NISP Optical Assembly (NI-OA), the NISP Detector System (NI-DS), and the NISP Warm Electronics (NI-WE).

Among its many components, NI-OA includes the Filter Wheel Assembly (FWA) and the Grism Wheel Assembly (GWA), allowing NISP to observe in photometric or spectroscopic mode, respectively [4].

NI-DS consists of sixteen Teledyne H2RG detectors (with a 2.3 µm cut-off) interfaced with the ASIC readout system [5]. The H2RG detectors are placed in the Focal Plane Array (FPA) to form a squared array in correspondence to the NISP's tilted focal plane. Each H2RG detector mounted on the NISP FPA is composed of an array of 2048 × 2048 pixels with 18 µm pitch. The pixel array consists of 2040 × 2040 regular photosensitive pixels, called "Science pixels", which collect the incoming photons through a nondestructive readout mode (see section 2.1). The array of Science pixels is surrounded by a four pixel–wide frame, called "Reference pixels". Reference pixels are designed to mimic the electronic behaviour of Science pixels while not being sensitive to light. For this reason, they are called "reference" pixels because they can be used to monitor the pixel array, ensuring its stability during signal acquisition. Moreover, Reference pixels are used in the NISP data processing to correct the scientific signal from electronic and temperature drift [6].

Finally, NI-WE is composed of one Instrument Control Unit (ICU) and two Data Processing Unit (DPU). The ICU is responsible for the commanding and the control of the instrument [7], while the DPUs manage the data acquisition, the onboard data processing, and the transfer of scientific data[8].

A detailed description of the NISP performance during the on-ground test and in-flight operations can be found respectively in [9] and [10].

2.1 The NISP Signal Detection Chain

NISP is designed to perform onboard scientific data processing. NISP's detectors acquire the signal by a nondestructive readout method so that the charge generated by photons is accumulated and sampled up the ramp (UTR) at a constant frame cadence of 1.45408 s. The readout pattern, commonly called MACC(n_g,n_f,n_d), is constituted by n_g groups, i.e., the average signal of n_f consecutive frames, separated by n_d dropped frames. The ASIC firmware allows NISP to acquire data in two different readout modes: the photometric MACC(4,16,4), and the spectroscopic MACC(15,16,11).

For each one of the sixteen H2RG detectors, the per-pixel UTR signal (Analog to Digital Unit (ADU)) is processed onboard by the two NISP DPUs. The DPU Application Software (ASW) [11] implements an ad-hoc signal estimator that measures the incoming flux through an analytical likelihood maximisation approach [12].

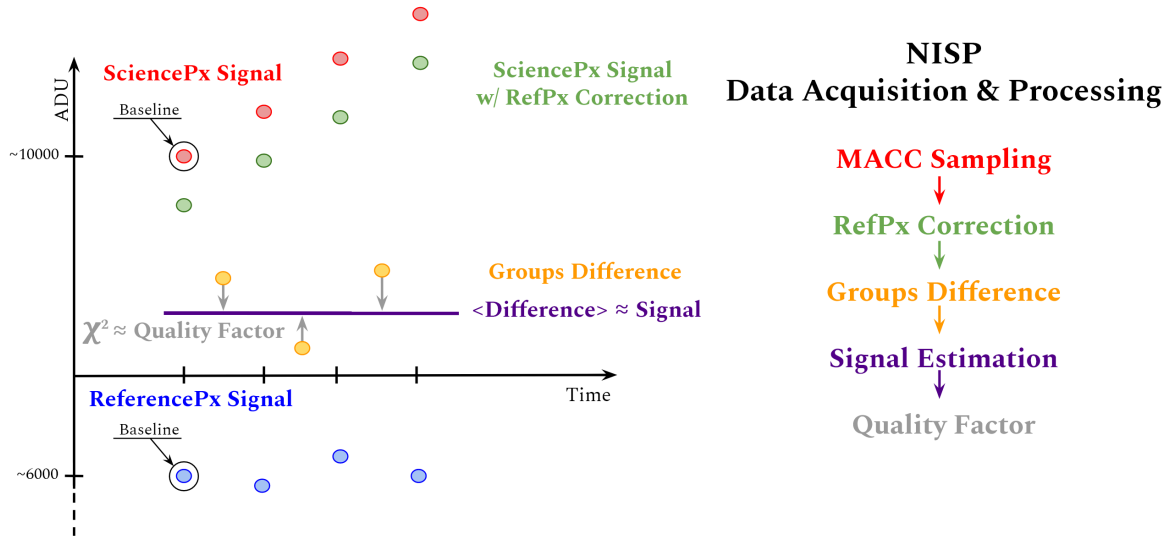

Figure 1: Schematic view (not to scale) of the NISP signal detection chain.

The reason for the onboard processing is mainly to reduce the amount of data to be downlinked to Earth. If UTR acquisitions were directly transmitted to Earth, the amount of NISP data would exceed the designed budget by more than 60 times [3].

Since only the measured flux is transmitted to Earth, the NISP signal detection chain provides a statistical estimator for the goodness of the fit. Following the likelihood maximisation approach, a robust technique, called Quality Factor (QF), was defined to identify any anomalies in the signal ramp, like non-linearity, cosmic rays, and random electrical effects [12]. The NISP QF map, downlinked together with the signal map, provides a measurement of the reliability of the estimated flux and is used in the data reduction and scientific analysis performed by the *Euclid* Science Ground Segment (SGS).

A schematic representation of the NISP signal detection chain is given in Fig. 1. The acquisition and processing of NISP signal can be summarized as follows:

1. The scientific signal is acquired by the H2RG detectors, with a MACC sampling approach, and it is corrected for the reference pixel's signal.
2. The differences of consecutive groups are computed to reduce the correlations between data points.
3. The NISP DPU ASW computes the integrated flux and the associated QF pixel maps.

More details on the acquisition and processing of NISP data can be found in [3], [6], [8], [11], and [12].

3. THE NISP COMMISSIONING PHASE

Immediately after the launch, the *Euclid*'s commissioning phase started at the European Space Operations Centre (ESOC/MOC Darmstadt, Germany). During the visibility periods ($\sim$ 12 hour per day), while the satellite was transiting to its final destination at the second Lagrange point (L_2) of the Earth-Sun system, the NISP temperature was monitored by the ICU. On July 6, at a temperature of about 210 K, the two DPUs were powered on and configured for flight operations, followed on July 13 by the FPA at an operating temperature of about 95 K. The commissioning of the *Euclid* spacecraft and instruments took about a month, after which an intensive six-month period was devoted to verifying scientific performance and deriving in-flight calibration. At last, in early February 2024, the Early Survey Operation began [13] [14], kicking off the survey that will probe the Universe across 10 billion years of cosmic expansion history.

3.1 NISP Baseline Calibration

The first activity performed during the NISP FPA's commissioning was the baseline adjustment, aiming to ensure every NISP acquisition settles into the most suitable range of differential non-linearity (DNL) [15] [16].

The baseline of H2RG detectors is essentially the pedestal value of the UTR acquisition, i.e., the first group in the MACC sampling approach. The baseline optimization ensures the best utilization of the dynamic range, i.e., the number of accumulated charges digitized by the ASIC readout electronics. It guarantees that non-linearity effects do not significantly alter the signal quality and it prevents, for example, the ramp from immediately going into saturation. The VRefMain is the ASIC bias establishing the main Pre–Amp reference input of the H2RG detector. Since the baseline depends on this bias, the VRefMain is used to adjust it.

During the on-ground test campaign (hereafter TV) of the NISP detectors, the dynamic range was optimized for each detector to obtain a reference benchmark at $\sim$ 90 K. This activity led to the definition of the optimized per detector default settings, which were loaded in the NISP DPU ASW before the launch. Therefore, when the NISP FPA was powered on during the commissioning phase, the VRefMain values determined during the TV campaign were used for the first setting of the detectors' baseline.

The temperature at which NISP stabilized during early flight operations ($\sim$ 94 K) was higher than the temperature achieved during the TV campaign. Because of its thermal sensitivity, such a temperature difference resulted in a shift of the baseline signal ($\sim$ 800 ADU on average), requiring further fine-tuning of the detectors' baseline. The procedure designed to measure the NISP detectors' baseline essentially consists of acquiring one dark MACC(1,16,1) image (without applying the reference pixel correction), computing the median value of the signal for reference and science pixels individually, and comparing those values to the TV references. Then, the tuning of the VRefMain bias, i.e., the voltage shift estimated through the Median–VRefMain conversion gains (ADU/V), is executed to match the reference values.

Because of the different operating temperatures, the conversion gains also had to be calibrated to achieve the most accurate baseline setting. Therefore, we performed a series of baseline measurements with different values of VRefMain to estimate the in-flight conversion gains. Figure 2 presents an example of the in-flight calibration of these conversion gains for one of the NISP detectors, identified by the SCA ID (SCA18XYZ) and its position (DETXY) in the NISP FPA. The circle shows the baseline measurements for different VRefMain values. The solid line presents a linear fit of the data points, whose slope gives an estimate of the conversion gain, while the TV calibration is shown with a dot-dashed line. Essentially, by calculating the angular coefficient in the Median–VRefMain plane, we derived a new set of conversion gains (ADU/V) that were then used to set the NISP detectors' baseline in its current configuration, as shown in Fig. 3.

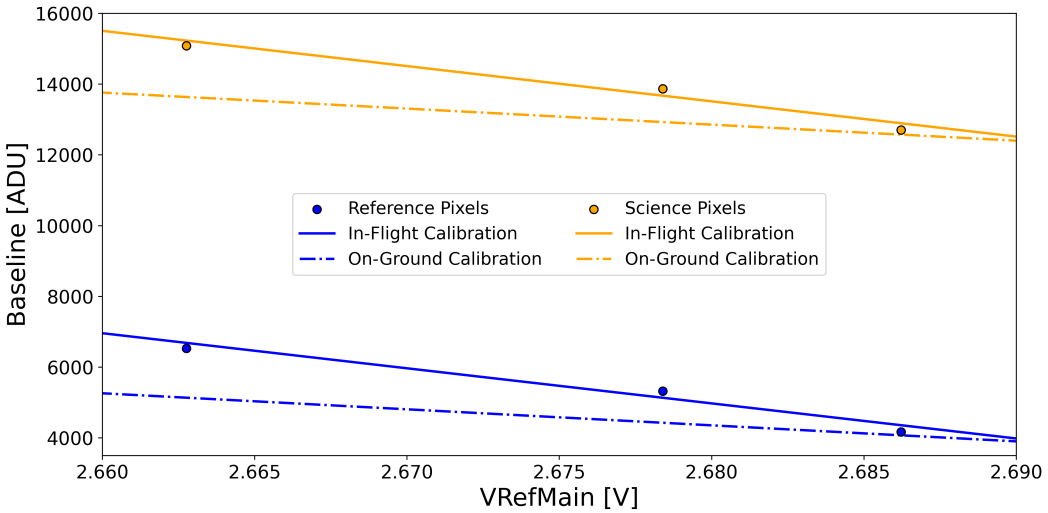

Figure 2: Example (DET42, SCA18249) of the in-flight (solid lines) and ground (dash-dot lines) calibration of the VRefMain conversion gain (ADU/V).

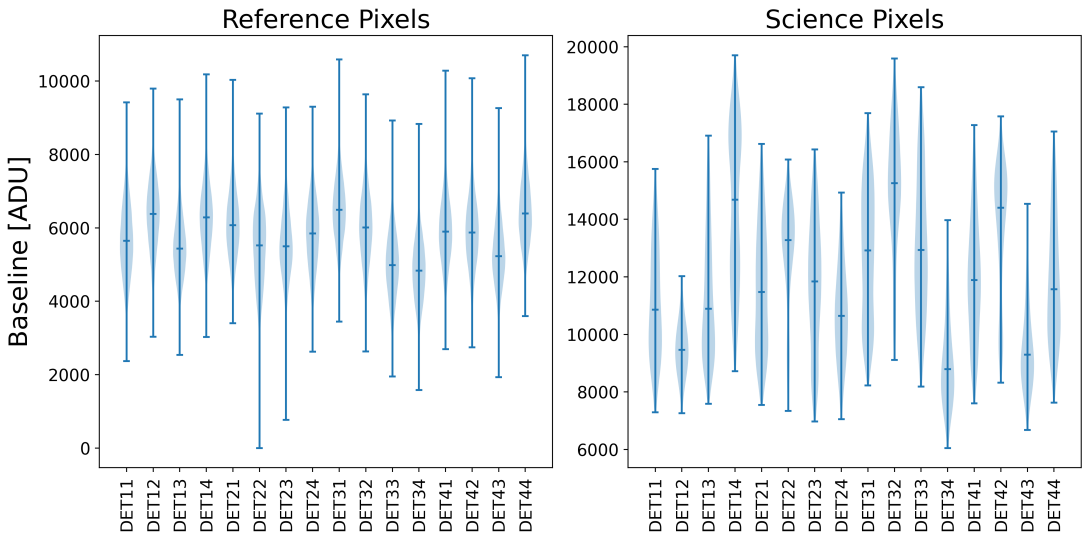

Figure 3: Final configuration of NISP FPA baseline. For each detector, the violin plots show the distribution of the signal acquired with a dark MACC(1,16,1). The left panel shows the Reference pixels' baseline distributions. The right one shows the Science pixels' baseline distributions within the 5th and 95th percentiles.

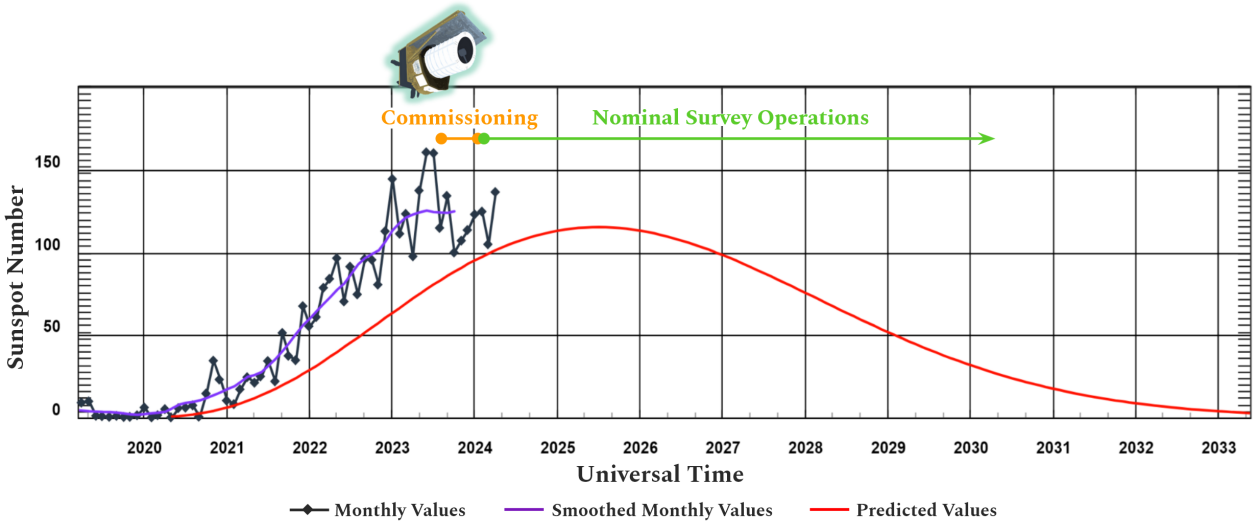

Figure 4: *Euclid*'s nominal lifetime compared to the foreseen sunspot number (red curve). Adapted from [17].

3.2 NISP Quality Factor vs. Solar proton flux

The cosmic rays (CRs) main population at L_2 is a mix of protons with Solar and Galactic origin, with the portion of Galactic protons strongly anti-correlated with the Solar activity's intensity [18]. Because *Euclid* is facing (and will face) the peak of the 25th Solar cycle for much of its operational time (see Fig. 4), this work focuses on the cosmic ray component produced by the Sun. In particular, we select the GOES satellite data [17] as the reference measurement of the Solar proton flux, hereafter GOES proton flux.

The light-sensitive substrate of the NISP H2RG detectors consists of a $Hg_{1-x}Cd_xTe$ layer about 2 µm thick, with a cadmium fraction $x = 0.54$. When a proton collides with the detector, it interacts electromagnetically with the atoms of the sensitive substrate, generating several electron-hole pairs. The intrinsic electric field E_{drift} of the pn-junction drives the holes toward the ReadOut Integrated Circuit (ROIC). As schematized in Fig. 5, this interaction introduces a spurious signal into the UTR acquisition, causing systematic errors in the flux estimation.

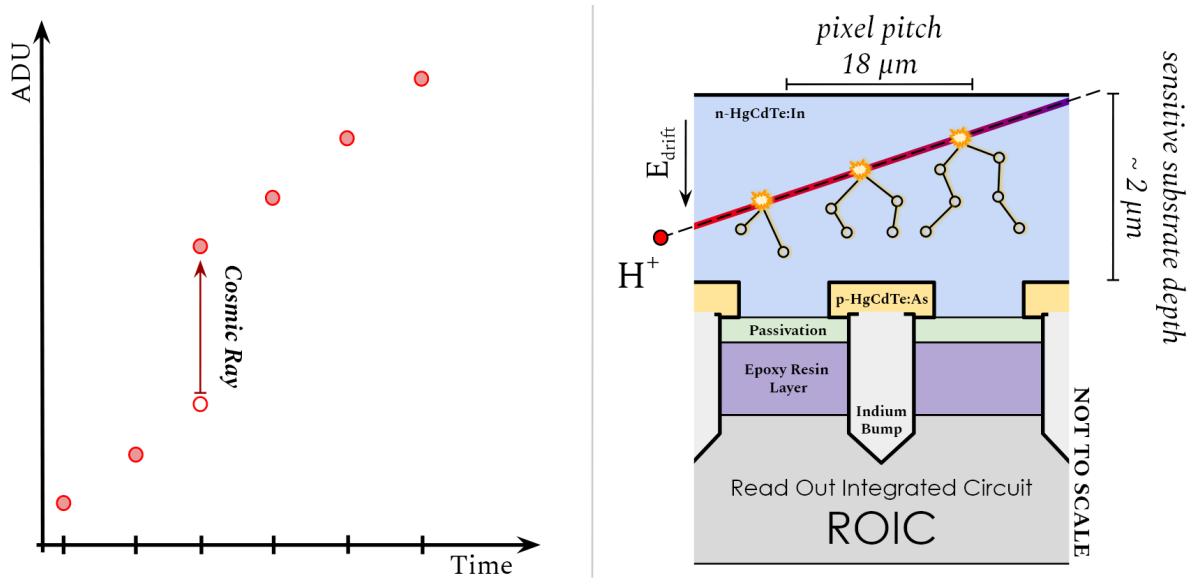

Figure 5: **Left:** Example of the effect on a single H2RG pixel of a cosmic ray hit during UTR acquisition. In particular, the cosmic ray releases charges in a dropped frame and the subsequent group signal is shifted accordingly. The measurements of the integrated group signal are shown with closed circles, with the open circle representing the expected group signal in the absence of CR hits. **Right:** Schematic representation of the physical interaction between a cosmic ray and the sensitive substrate of an H2RG detector, adapted from [19]. Holes induced by CR interaction are shown with empty circles, while electrons are not shown. Black lines connecting empty circles show the path of a single hole toward the p-type HgCdTe.

Since the QF method is designed to detect any possible deviation from the linear assumption of the NISP signal integration, it is a key tool for estimating the number of CRs interacting with NISP detectors. The performance of the QF and its responsiveness in identifying CR hits in UTR measurements were thoroughly investigated during the NISP test campaigns [20]. Since the NISP signal is estimated through the difference of groups [12], the QF revealed the peculiar property of increasing its value when the pixel is affected by a CR, regardless of the position of the hit in the UTR sampling.

During the first flight operations of *Euclid*, several coronal mass ejection events were measured, leading to a significant increase in the Solar proton flux hitting the NISP detectors. Specifically, a prolonged, high-intensity proton flare in March 2024 affected the NISP operations due to unexpected delays in the transmission of science data to the spacecraft's mass memory unit [21]. This type of event highlights the impact of space weather on the performance of L_2–based instruments and led to the preliminary analysis of the correlation between Solar proton flux and *Euclid*'s NISP measurements performed in this paper.

The analysis of the NISP spectroscopic observations from February to April 2024 revealed interesting insights into the response of the NISP QF distribution to Solar activity and, specifically, to the variation of GOES proton flux. Figure 6 illustrates that the higher the proton flux intensity, the higher the number of pixels reporting QF $\gtrsim 30$. Consequently, a threshold value of QF $= 30$ was established to identify pixels hit by cosmic rays. This approach led to defining the number of pixels with QF > 30 as a proxy for the number of CRs affecting NISP observations, hereafter NISP QF Proxy. Hence, the time evolution of the NISP QF Proxy can be compared to the GOES satellite data to study possible correlations between the NISP QF response and the flux of Solar protons for different energy ranges. Specifically, using data produced by the GOES primary and secondary spacecraft from March 15 to March 19, 2024, we focused the analysis on three different energy ranges, namely, $5-10$ MeV, $10-30$ MeV, and >30 MeV. From Fig. 7, it is immediately evident that the changes in the flux of protons with $E > 30$ MeV are strongly correlated with those of the NISP QF Proxy, while this is not true in the $5-10$ MeV and $10-30$ MeV cases. In fact, in the lower energy cases, the structure of multiple intensity peaks observed by GOES does not match the time evolution of the NISP QF Proxy.

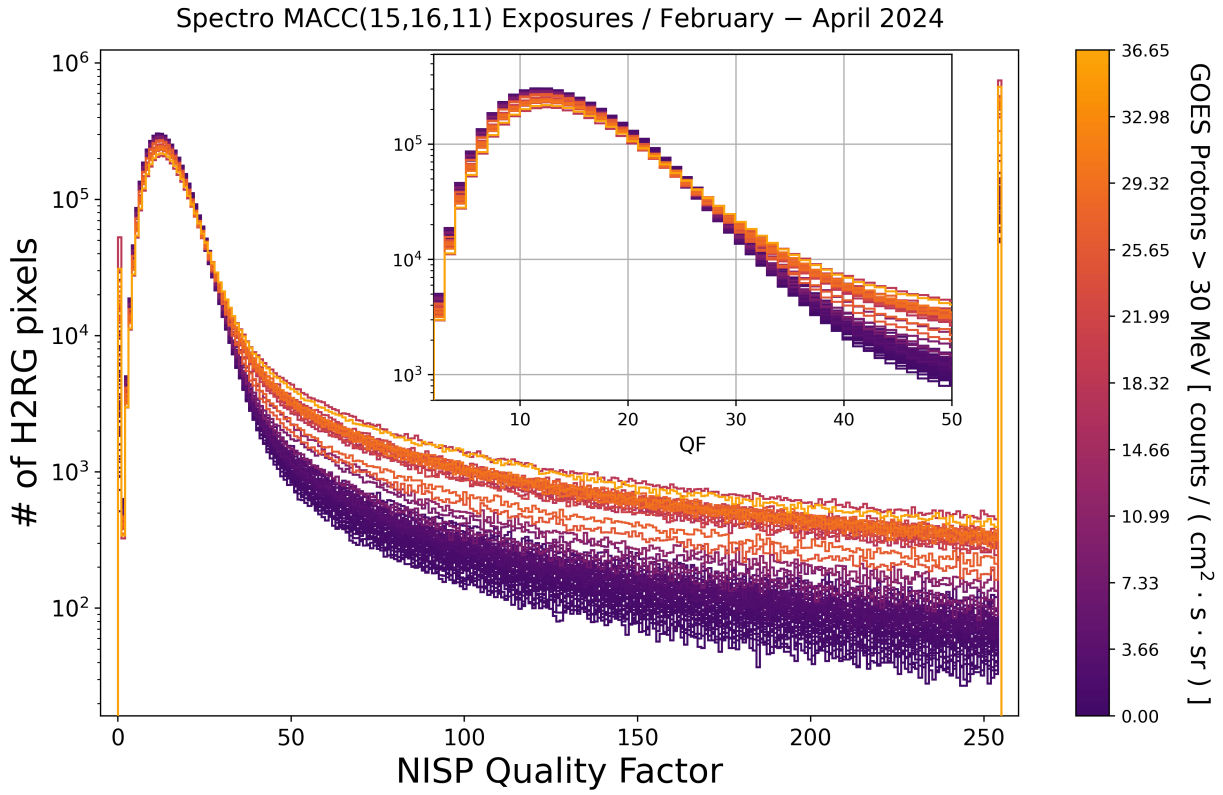

Figure 6: Example of the variations induced in the NISP QF distributions by different GOES proton flux intensities ($E > 30$ MeV).

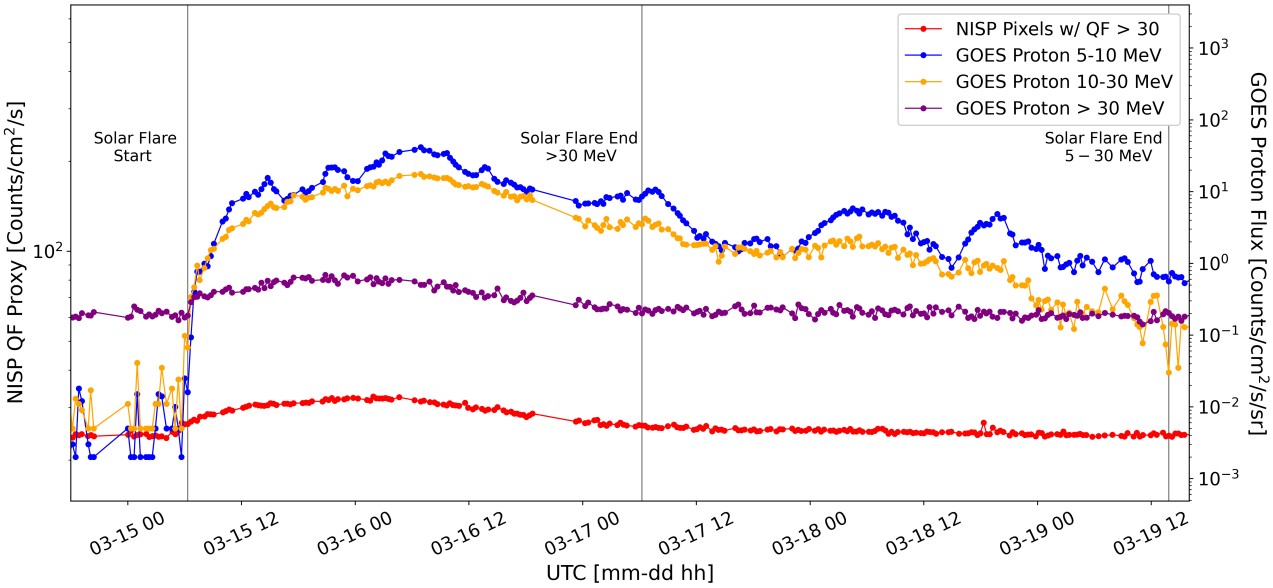

Figure 7: Comparison of the time evolution of NISP QF Proxy and GOES data during the March 2024 Solar flare. The blue, yellow, and purple data points report the Solar proton flux in different energy ranges, while the NISP measurements are reported in red. Because of the different physical units, the evolution of the NISP QF Proxy refers to the left axis, while the GOES proton flux refers to the right one.

A more robust and statistically significant confirmation of this hypothesis can be obtained by applying the two–sample Kolmogorov–Smirnov (KS) Test to the cumulative distribution functions (CDF) of the various observables, i.e., NISP QF Proxy and GOES proton flux as a function of proton energy. In the case of NISP, the null hypothesis wants to test whether or not NISP QF Proxy and GOES proton flux are following the same time evolution, and if this hypothesis depends on the particles' energy.

In practice, for each energy range, the cumulative counts of NISP QF Proxy and GOES proton flux are calculated within a time window defined so that the GOES data undergoes a complete cycle, i.e., from minimum to minimum (see Fig. 7). The basic assumption of this approach is that if the NISP QF is responsive to Solar activity, then a change in GOES proton flux will also be observed by the NISP QF Proxy. Therefore, through the time correlation between GOES data and NISP QF Proxy, we aim to determine the energy of protons to which NISP is actually sensitive.

Table 1 reports the results of the KS test, in addition to the detail of the selected time windows, while Fig. 8 shows the comparison between the CDF of NISP QF Proxy and GOES data. The p–values from the KS test strongly indicate that NISP is only sensitive to protons with energies above 30 MeV, as the correlations with protons at $5-10\,\mathrm{MeV}$ and $10-30\,\mathrm{MeV}$ are rejected with a confidence level of more than 99%.

Table 1: Results of the two–sample Kolmogorov-Smirnov Test applied to NISP QF Proxy and GOES proton flux for three different ranges of particle energy.

Proton Energy	**Solar Flare Timing**		**Kolmogorov–Smirnov Test**		
MeV	Start	End	p–value	statistic	null–hypothesis
$5-10$	2024–03–15	2024–03–19	5.39×10^{-14}	0.36	rejected
$10-30$	2024–03–15	2024–03–19	4.15×10^{-17}	0.40	rejected
>30	2024–03–15	2024–03–17	0.82	0.09	accepted

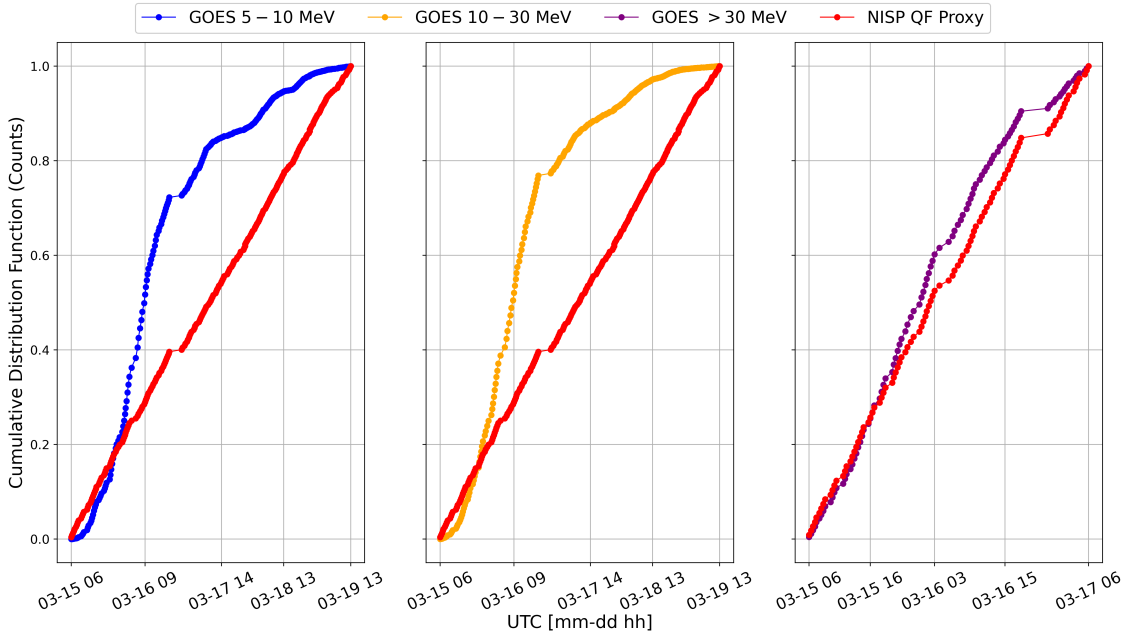

Figure 8: Comparison between CDF of NISP QF Proxy and GOES data for different proton energy ranges from the lowest to the highest energy bin from left to right. The time window within which the CDF is computed varies according to Tab. 1.

Since the NISP detectors are shielded inside the *Euclid* spacecraft, the lowest-energy protons are expected to be completely absorbed by the surrounding material. Specifically, the equivalent shielding for NISP FPA was estimated to be around $1.1 - 1.5\,\mathrm{cm}$ of Aluminium, whose corresponding stopping power matches our findings. Furthermore, looking at the literature concerning other space missions operating in L_2, it is possible to verify how a similar result has already been observed by the ESA *Planck* mission [22].

To observe that the QF is indeed able to monitor the actual cosmic ray flux incident on the detectors is certainly a noteworthy achievement that further consolidates the role of the QF as a method of verifying the quality of the NISP signal, which is estimated onboard *Euclid* at a distance of 1.5 million kilometres from Earth.

4. CONCLUSIONS

The commissioning phase of the NISP instrument, onboard the ESA's *Euclid* mission, has yielded significant insights into its performance and calibration requirements.

The calibration of the NISP detectors' baseline was a critical task to ensure the optimal performance of the signal detection chain. The initial ground-based settings had to be adjusted due to the different operating conditions of the detectors in space. This process included measuring the baseline using dark MACC(1,16,1) images and recalibrating conversion gains, see Fig. 2 and Fig. 3. The success of this calibration ensures that the NISP detectors can effectively use their dynamic range, minimizing differential non-linearity effects.

The Quality Factor method proved to be a robust tool for monitoring the temporal evolution of cosmic rays flux at L_2. During periods of high Solar activity, like the one in which *Euclid* operates, the main source of cosmic rays acting in L_2 is the ejection of charged particles emitted by the Sun in the so-called coronal mass ejection events. Analyzing the data collected during the first flight operations of NISP, a strong correlation is detected between the time profiles of the NISP QF and the flux of high-energy Solar protons ($E > 30$ MeV). For example, during the flare event of mid-March, the NISP QF Proxy – i.e., the number of pixels with QF > 30 – closely follows the time evolution of the flux of Solar protons with energies above 30 MeV, see Fig. 7, Fig. 8, and Table 1. The outcomes of this analysis are consistent with the equivalent shielding of NISP FPA, confirming the excellent performance of the Quality Factor in identifying the effects of charged particles on the data processing performed onboard by the NISP Data Processing Unit.

Successfully calibrating and understanding the performance of the NISP instrument under different operating conditions is a crucial step toward the primary goal of the mission. As *Euclid* proceeds with the survey, continuous monitoring and calibration campaigns of the instruments will be essential to account for hardware degradation and space environment variability and ensure the highest quality of scientific data. Lessons learned from the commissioning phase will guide these efforts, supporting *Euclid* over its operational lifetime.

ACKNOWLEDGMENTS

The authors would like to thank all the people involved in the design, building, development and commissioning of *Euclid* for their efforts and dedication that made this work possible. The Euclid Consortium acknowledges the European Space Agency and a number of agencies and institutes that have supported the development of *Euclid*, in particular the Academy of Finland, the Agenzia Spaziale Italiana, the Belgian Science Policy, the Canadian Euclid Consortium, the French Centre National d'Etudes Spatiales, the Deutsches Zentrum für Luft- und Raumfahrt, the Danish Space Research Institute, the Fundação para a Ciência e a Tecnologia, the Ministerio de Ciencia e Innovación, the National Aeronautics and Space Administration, the National Astronomical Observatory of Japan, the Netherlandse Onderzoekschool Voor Astronomie, the Norwegian Space Agency, the Romanian Space Agency, the State Secretariat for Education, Research and Innovation (SERI) at the Swiss Space Office (SSO), and the United Kingdom Space Agency. A complete and detailed list is available on the *Euclid* web site (`http://www.euclid-ec.org`). The involvement of F. Cogato and E. Medinaceli in the SPIE Astronomical Telescopes + Instrumentation 2024 conference was funded by the INAF Programma di Ricerca Fondamentale 2023 - MiniGrant RSN5.

References

[1] Euclid Collaboration and Mellier, Y., et al., "Euclid. I. Overview of the Euclid mission," *arXiv e-prints* , arXiv:2405.13491 (May 2024).

[2] Euclid Collaboration and Cropper, M., et al., "Euclid. II. The VIS Instrument," *arXiv e-prints* , arXiv:2405.13492 (May 2024).

[3] Euclid Collaboration and Jahnke, K., et al., "Euclid. III. The NISP Instrument," *arXiv e-prints* , arXiv:2405.13493 (May 2024).

[4] Grupp, F., Kaminski, J., Bodendorf, C., Geis, N., Penka, D., and Bender, R., "Euclid warm testing of the near-infrared optical assembly using a unique combination of CGH interferometry and tactile precision measurements," in [*Astronomical Optics: Design, Manufacture, and Test of Space and Ground Systems II*], Hull, T. B., Kim, D. W., and Hallibert, P., eds., *Society of Photo-Optical Instrumentation Engineers (SPIE) Conference Series* **11116**, 1111618 (Sept. 2019).

[5] Crouzet, P. E., ter Haar, J., de Wit, F., Beaufort, T., Butler, B., Smit, H., van der Luijt, C., and Martin, D., "Characterization of HAWAII-2RG detector and SIDECAR ASIC for the Euclid mission at ESA," in [*High Energy, Optical, and Infrared Detectors for Astronomy V*], Holland, A. D. and Beletic, J. W., eds., *Society of Photo-Optical Instrumentation Engineers (SPIE) Conference Series* **8453**, 84531R (July 2012).

[6] Kubik, B., Barbier, R., Castera, A., Chabanat, E., Ferriol, S., and Smadja, G., "Impact of common modes correlations and time sampling on the total noise of a H2RG near-IR detector," in [*High Energy, Optical, and Infrared Detectors for Astronomy VI*], Holland, A. D. and Beletic, J., eds., *Society of Photo-Optical Instrumentation Engineers (SPIE) Conference Series* **9154**, 91541B (July 2014).

[7] Ligori, S., Corcione, L., Capobianco, V., Bonino, D., Sirri, G., Valieri, C., Giacomini, F., Patrizii, L., Valenziano, L., Auricchio, N., Davini, S., Di Domizio, S., Dusini, S., Caminata, A., Testera, G., and Tosi, S., "The application software for the instrument control unit of the NISP instrument of the Euclid mission: final status and lessons learned after delivery of the flight version," in [*Space Telescopes and Instrumentation 2020: Optical, Infrared, and Millimeter Wave*], Lystrup, M. and Perrin, M. D., eds., *Society of Photo-Optical Instrumentation Engineers (SPIE) Conference Series* **11443**, 114435B (Dec. 2020).

[8] Medinaceli, E., Farinelli, R., Balestra, A., Sirignano, C., Dusini, S., Veri, C., Valenziano, L., Auricchio, N., Battaglia, P., Franceschi, E., and Stanco, L., "Data processing unit's hardware and application software description of the Near Infrared Spectro-Photometer: Euclid mission," in [*Space Telescopes and Instrumentation 2020: Optical, Infrared, and Millimeter Wave*], Lystrup, M. and Perrin, M. D., eds., *Society of Photo-Optical Instrumentation Engineers (SPIE) Conference Series* **11443**, 1144359 (Dec. 2020).

[9] Maciaszek, T., Ealet, A., and Gillard, W., et al., "Euclid near infrared spectrometer and photometer instrument flight model presentation, performance, and ground calibration results summary," in [*Space telescopes and instrumentation 2022: Optical, infrared, and millimeter wave*], Coyle, L. E., Matsuura, S., and Perrin, M. D., eds., **12180**, 121801K, SPIE (2022). International Society for Optics and Photonics.

[10] Gillard, W. et al., "Euclid Near Infrared Spectrometer and Photometer instrument in space," *Society of Photo-Optical Instrumentation Engineers (SPIE) Conference Series* , 13092–23 (June 2024).

[11] Bonoli, C., Balestra, A., Bortoletto, F., D'Alessandro, M., Farinelli, R., Medinaceli, E., Stephen, J., Borsato, E., Dusini, S., Laudisio, F., Sirignano, C., Ventura, S., Auricchio, N., Corcione, L., Franceschi, E., Ligori, S., Morgante, G., Patrizii, L., Sirri, G., Trifoglio, M., and Valenziano, L., "On-board data processing for the near infrared spectrograph and photometer instrument (NISP) of the EUCLID mission," in [*Space Telescopes and Instrumentation 2016: Optical, Infrared, and Millimeter Wave*], MacEwen, H. A., Fazio, G. G., Lystrup, M., Batalha, N., Siegler, N., and Tong, E. C., eds., *Society of Photo-Optical Instrumentation Engineers (SPIE) Conference Series* **9904**, 99045R (July 2016).

[12] Kubik, B., Barbier, R., and Chabanat, E., et al., "A New Signal Estimator from the NIR Detectors of the Euclid Mission," *PASP* **128**, 104504 (Oct. 2016).

[13] Laureijs, R. J. et al., "Euclid mission: first year of operations," *Society of Photo-Optical Instrumentation Engineers (SPIE) Conference Series* , 13173–504 (June 2024).

[14] Vavrek, R. et al., "The Euclid mission: status after launch and early operations ," *Society of Photo-Optical Instrumentation Engineers (SPIE) Conference Series* , 13092–21 (June 2024).

[15] Barbier, R., Buton, C., Clemens, J. C., Conversi, L., Ealet, A., Ferriol, S., Fornari, F., Gillard, W., Kohley, R., Kubik, B., Rosset, C., Secroun, A., Serra, B., Smadja, G., and Zoubian, J., "Detector chain calibration strategy for the Euclid flight IR H2RGs," in [*High Energy, Optical, and Infrared Detectors for Astronomy VIII*], Holland, A. D. and Beletic, J., eds., *Society of Photo-Optical Instrumentation Engineers (SPIE) Conference Series* **10709**, 107090S (July 2018).

[16] Waczynski, A., Barbier, R., Cagiano, S., Chen, J., Cheung, S., Cho, H., Cillis, A., Clémens, J. C., Dawson, O., Delo, G., Farris, M., Feizi, A., Foltz, R., Hickey, M., Holmes, W., Hwang, T., Israelsson, U., Jhabvala, M., Kahle, D., Kan, E., Kan, E., Loose, M., Lotkin, G., Miko, L., Nguyen, L., Piquette, E., Powers, T., Pravdo, S., Runkle, A., Seiffert, M., Strada, P., Tucker, C., Turck, K., Wang, F., Weber, C., and Williams, J., "Performance overview of the Euclid infrared focal plane detector subsystems," in [*High Energy, Optical, and Infrared Detectors for Astronomy VII*], Holland, A. D. and Beletic, J., eds., *Society of Photo-Optical Instrumentation Engineers (SPIE) Conference Series* **9915**, 991511 (July 2016).

[17] GOES, "University of colorado boulder and space weather technology, research, and education center, "swx trec space weather data portal." laboratory for atmospheric and space physics," (2019). https://doi.org/10.25980/NMFX-XX89.

[18] Catalano, A., Ade, P., Atik, Y., Benoit, A., Bréele, E., Bock, J. J., Camus, P., Chabot, M., Charra, M., Crill, B. P., Coron, N., Coulais, A., Désert, F. X., Fauvet, L., Giraud-Héraud, Y., Guillaudin, O., Holmes, W., Jones, W. C., Lamarre, J. M., Macías-Pérez, J., Martinez, M., Miniussi, A., Monfardini, A., Pajot, F., Patanchon, G., Pelissier, A., Piat, M., Puget, J. L., Renault, C., Rosset, C., Santos, D., Sauvé, A., Spencer, L. D., and Sudiwala, R., "Impact of particles on the Planck HFI detectors: Ground-based measurements and physical interpretation," **A&A, 569**, A88 (Sept. 2014).

[19] Mosby, G., Rauscher, B. J., Bennett, C., Cheng, E. S., Cheung, S., Cillis, A., Content, D., Cottingham, D., Foltz, R., Gygax, J., Hill, R. J., Kruk, J. W., Mah, J., Meier, L., Merchant, C., Miko, L., Piquette, E. C., Waczynski, A., and Wen, Y., "Properties and characteristics of the Nancy Grace Roman Space Telescope H4RG-10 detectors," *Journal of Astronomical Telescopes, Instruments, and Systems* **6**, 046001 (Oct. 2020).

[20] Kubik, B., Barbier, R., Calabria, P., Castera, A., Chabanat, E., Charlieu, F., Clemens, J.-C., Ealet, A., Ferriol, S., Gillard, W., Maciaszek, T., Prieto, E., Schirra, F., Secroun, A., Serra, B., Smadja, G., Tilquin, A., and Zoubian, J., "Low noise flux estimate and data quality control monitoring in EUCLID-NISP cosmological survey," in [*Space Telescopes and Instrumentation 2016: Optical, Infrared, and Millimeter Wave*], MacEwen, H. A., Fazio, G. G., Lystrup, M., Batalha, N., Siegler, N., and Tong, E. C., eds., *Society of Photo-Optical Instrumentation Engineers (SPIE) Conference Series* **9904**, 99045J (July 2016).

[21] Battaglia, P. M. et al., "Euclid: the Near Infrared Spectrometer and Photometer (NISP) instrument operations," *Society of Photo-Optical Instrumentation Engineers (SPIE) Conference Series* , 13092–240 (June 2024).

[22] Planck Collaboration and Ade, P. A. R., et al., "Planck 2013 results. x. hfi energetic particle effects: characterization, removal, and simulation," **A&A, 571**, A10 (Nov. 2014).